Properties of TiN/TiCN multilayer films by direct current magnetron sputtering

2012 J. Phys. D: Appl. Phys. 45 095303

(http://iopscience.iop.org/0022-3727/45/9/095303)

IOP PUBLISHING JOURNAL OF PHYSICS D: APPLIED PHYSICS

J. Phys. D: Appl. Phys. **45** (2012) 095303 (9pp) doi:10.1088/0022-3727/45/9/095303

Properties of TiN/TiCN multilayer films by direct current magnetron sputtering

Jianyun Zheng[1,2], **Junying Hao**[1], **Xiaoqiang Liu**[1,2] **and Weimin Liu**[1]

[1] State Key Laboratory of Solid Lubrication, Lanzhou Institute of Chemical Physics, Chinese Academy of Sciences, Lanzhou 730000, People's Republic of China
[2] Graduate University of Chinese Academy of Sciences, Beijing 100049, People's Republic of China

E-mail: jyhao@licp.cas.cn

Received 2 October 2011, in final form 29 December 2011
Published 20 February 2012
Online at stacks.iop.org/JPhysD/45/095303

Abstract

In this work, a TiN/TiCN multilayer film was deposited by direct current magnetron sputtering. Its thickness was about 9675 nm and the bilayer numbers were 10. The composition, crystalline structure and amorphous carbon (a-C) phase of the film were investigated by x-ray photoelectron spectroscopy, x-ray diffraction and Raman spectroscopy. Field emission scanning electron microscopy was employed to observe the inner structure of the film. The TiCN layer exhibited a glass-like structure and the TiN layer presented a columnar structure. The adhesion force between the film and the substrate was 37.8 N determined by scratch tests. The hardness of the uppermost TiCN layer and the total film was 34.22 GPa and 27.22 GPa obtained by nano-indentation tests, respectively. In addition, the TiN/TiCN multilayer thick film showed different types of tribological behaviour against Si_3N_4 balls and steel balls. The mean coefficient of friction and the wear rate of the film were about 0.14 and 1.15×10^{-6} mm^3 N^{-1} m^{-1} when the film slid against Si_3N_4 balls for 1 h.

(Some figures may appear in colour only in the online journal)

1. Introduction

Surface modification using hard films as a surface engineering process has long been proven to be an outstandingly successful way. Multilayer structure hard films have recently drawn wide attention of researchers, who attempted to further improve the properties of the multilayer films based on the traditional single layer films (Barshilia *et al* 2005, Miao *et al* 2007, Chang and Chang 2009, Polcar *et al* 2009). Among various multilayer hard films, films containing Ti compounds (TiN/CN, TiN/TiCN, TiN/TiC, Ti/TiN) have most frequently been investigated in the past decade. For example, Morant *et al* (2004) studied the enhancement of hardness achieved by depositing an elastic film (CN) on hard layers (TiN/TiCN). Bemporad *et al* (2001) obtained TiN/TiCN multilayer hard films grown on tool steels by the cathodic arc method. They indicated that the multilayer film configuration can optimize the interactions of the film/substrate as well as the film/working materials by controlling the internal stress state, fatigue toughness, hardness and superficial composition of these TiN/TiCN films. Furthermore, Agudelo *et al* (2008) reported the synthesis of Ti/TiN/TiCN multilayer films grown in graded form by dc sputtering. In fact, TiN/TiCN multilayer hard films still have numerous unexplored potential structures and properties, and are worth studying. Thus, in order to further improve the structure and properties, studies on thick TiN/TiCN multilayer films are necessary.

The aim of this work is to investigate the characteristics of thick TiN/TiCN multilayer films, as it is expected that the films combine the advantages of single layer films and those of multilayer thick films.

2. Experimental details

2.1. Specimen preparation

N-type Si (1 0 0) wafers with surface roughness of 20 nm were used as the substrate materials. The TiN/TiCN multilayer film was deposited by a direct current magnetron sputtering (dcMS) system (SKY Technology Development Co., Ltd, JS-650) sputtering titanium target (purity >99.5 wt%) in Ar (99.99%), N_2 (99.99%) and CH_4 (99.99%) mixed atmosphere.

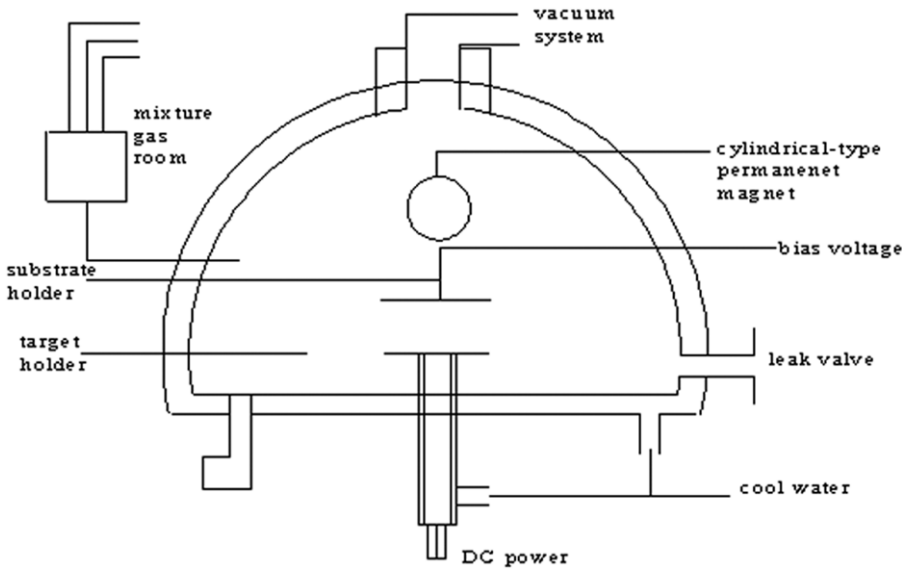

Figure 1. Top view of the dcMS system.

Table 1. Deposition conditions to produce the films.

Deposition parameter	Values
Deposition voltage	340–350 V
Current	4 A
Deposition pressure	0.21–0.25 Pa
Target–substrate distance	11.5 cm
Gases	Ar, N_2 and CH_4

The schematic diagram of the deposition system is shown in figure 1. Prior to loading into the chamber, all substrates were ultrasonically cleaned in acetone for 20 min. The deposition system was evacuated to a base pressure below 7×10^{-4} Pa before feeding Ar into the deposition chamber. Before deposition, the substrates were cleaned by Ar^+ bombardment for 10 min at a pressure of 1.7 Pa with a pulsed substrate bias voltage of −1100 V, to remove the thin oxide layer and other adherent impurities on Si wafers. Thereafter, direct current power was charged on the metal titanium target and the films were deposited. Details of the deposition conditions are listed in table 1 and the different CH_4 flow rates as well as the alternate cycles of TiN layer and TiCN layer are shown in table 2. In order to enhance the adhesion force between the film and the substrate, a Ti buffer layer was deposited on the Si wafer before the growth of the TiN/TiCN multilayer film (Kim *et al* 2003a), and the graded transition in the interface region was used (Monaghan *et al* 1993).

2.2. Film characterization

The chemical composition of the film was analysed by x-ray photoelectron spectroscopy (XPS) with monochromated Al Kα radiation at a pass energy of 29.4 eV. X-ray diffraction (XRD) measurement was used to characterize the crystalline structure of the film on a Philips X'perts diffractometer using Cu Kα radiation. In order to determine the existence of a-C phase in the film, a HR800 Raman microscope instrument was used with 532 nm Ar ion laser and a resolution of 1 cm^{-1}.

Table 2. Variation of CH_4 flow rates to obtain the TiN/TiCN multilayer film.

Ar flow rate (sccm)	N_2 flow rate (sccm)	CH_4 flow rate (sccm)	Time (min)	Phase	Bilayer numbers
20	0→6	0	6	Ti→TiN	
20	6	0	2	TiN	
20	6	0→10	1.5	TiN→TiCN	
20	6	10	3	TiCN	1
20	6	10→0	1.5	TiCN→TiN	
20	6	0	2	TiN	
20	6	0→10	1.5	TiN→TiCN	
20	6	10	3	TiCN	2
—	—	—	—	—	—
20	6	10→0	1.5	TiCN→TiN	
20	6	0	6	TiN	
20	6	0→10	1.5	TiN→TiCN	
20	6	10	18.5	TiCN	10

The surface image of the film was obtained in atomic force microscopy contact (AFM-C) mode with a scanning speed of 1 Hz and 256 × 256 pixels. The fractured cross-section and thickness of the film were observed using field emission scanning electron microscopy (FESEM, JSM-6701F).

2.3. Mechanical properties

Scratch tests were used to measure the adhesion force of the total film with a loading rate of 30 N min^{-1} by a scratch tester (Kaihua MFT-4000). The critical load and the adhesion failure were identified when the curve of friction versus load had a sudden shift. The hardness and elastic modulus were measured using a nano-indenter (Nanotest 600) with a Berkovich diamond tip. The mean value of hardness and elastic modulus of the film were obtained from the loading–unloading curves over three times. The indentation depth was about 10% of the film or layer thickness in order to reduce the influence of substrates or other layers (Graca *et al* 2011).

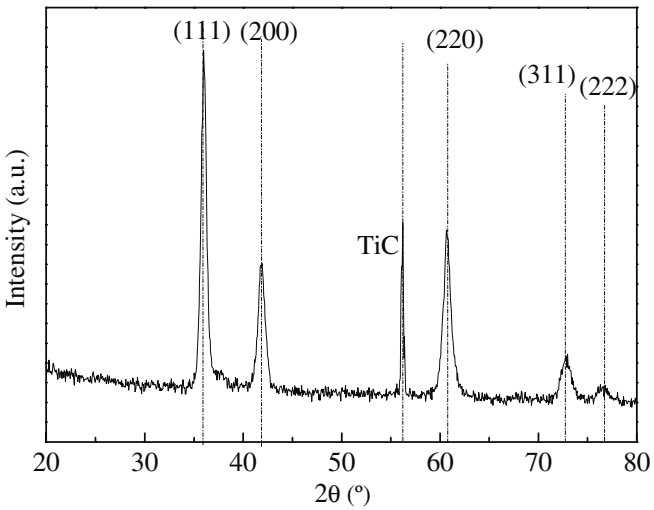

Figure 2. XRD pattern of the TiN/TiCN multilayer film.

2.4. Tribological properties

The tribological behaviour of the film was evaluated by a UMT-2MT tribometer (Center for Tribology, Inc., CA, USA) at room temperature of about 20 ± 5 °C and relative humidity of 40 ± 5%. Si_3N_4 balls and AISI52100 steel balls were used as the counterparts with a diameter of 3 mm and a surface roughness of 20 nm. Their hardness values were 850 HV and 1600 HV, respectively. All the tests were done at a sliding speed of 600 rpm and a load of 1.0 N. The sliding stroke was about 5 mm. After the tribological tests, the feature of wear track in the TiN/TiCN multilayer film was surveyed by a scanning electron microscope (SEM) (JSM-5600LV) with a resolution of 3.5 nm. A Micro XAM-3D surface profiler was used to observe the depth and width of the wear track and calculate the wear volume. Then the wear rate was obtained with the following equation (Oh *et al* 2003):

$$Ws = V/NS, \tag{1}$$

where V, N and S denote the wear volume, normal loads and the sliding distance, respectively. The component content of wear debris was evaluated by energy dispersive x-ray spectroscopy (EDS).

3. Results and discussion

3.1. Film structure

A typical XRD pattern of the TiN/TiCN multilayer film is shown in figure 2. All peaks corresponding to the (1 1 1), (2 0 0), (2 2 0), (3 1 1), (2 2 2) plane of the cubic $TiC_{0.7}N_{0.3}$ phase and TiC (2 2 0) phase are observed in the multilayer film. When TiC or TiCN is formed by introducing CH_4, it is difficult to find the diffraction peaks of the TiN phase (Tu *et al* 2011). Moreover, the peaks of the TiCN phase shift to lower angles (Klemberg-Sapieha *et al* 2007) and is close to the TiC phase since the C relative contents reach around 60 at% measured by XPS. This is ascribed to the substitution of N atoms with the bigger C atoms in the solid solution. Moreover, the multilayer film exhibits a strong (1 1 1) preferred orientation. This implies that the film structure is dense because the plane (1 1 1) orientation is the densely packed plane (Antunes *et al* 2010). Using the Sherrer equation (Klug and Alexander 1974), the average crystal size of the surface TiCN layer is estimated to be 14.6 nm. These results will be confirmed in the following section.

Figure 3 presents the XPS spectra of Ti 2p, N 1s and C 1s of the TiN/TiCN multilayer film. In the Ti spectrum, two peaks of Ti $2p_{3/2}$ are found at 454.3 and 455.7 eV. According to Louw *et al* (1991), the Ti $2p_{3/2}$ position of TiN films deposited by PVD is at 455.0 eV. The weak electronegative element C involves in the TiN/TiCN multilayer film formation, and that would slightly increase the binding energies of Ti–N (Shi *et al* 2000). Thus, the 454.3 eV and 455.7 eV peaks correspond to the Ti–C bonds and Ti–N bonds, respectively. The N 1s spectrum exhibits a peak at 396.5 eV, which corresponds to the N–Ti bonds. Cheng *et al* (2010) also found that the binding energy of the N 1s spectra of the TiCN films was lower than that of the TiN films. The C 1s spectrum consists of three peaks at binding energies of 281.5, 284.1 and 285.2 eV. The peak at 281.5 eV is assigned to the Ti–C bonds (Meng *et al* 2006). The peaks at 284.1 eV and 285.2 eV are assigned to the sp^2–C and sp^3–C bonds, respectively (Jiang *et al* 2010). The C 1s binding energies of pure graphite (284.3 eV) and diamond (285.3 eV) measured under the same conditions are cited for comparison.

It can also be seen from figure 3 that the peak at 281.5 eV occupies only a small fraction of the total C 1s spectrum compared with the other peaks, indicating that a small fraction of C atoms are bonded to Ti atoms, and most of the C atoms exist as amorphous carbon. A similar result was further obtained by Raman spectroscopy. Additionally, the composition would significantly affect the mechanical and tribological properties of the TiN/TiCN multilayer film.

Similarly, Raman spectroscopy also can determine the a-C phase of TiN/TiCN multilayer films (Irmer and Dorner-Reisel 2005). Usually, the Raman spectra of a-C : H films are characterized by a graphitic band (G-band) around 1540 cm^{-1} and disordered band (D-band) around 1370 cm^{-1} in the spectral region within 1000–1800 cm^{-1}. Details of the G- and D-peaks of a-C : H films are reported elsewhere (Ogwu *et al* 1999). The Raman spectrum of the TiN/TiCN multilayer film is given in figure 4. As seen in figure 4, six peaks were found. Among them, the peaks at 242, 352, 535 and 606 cm^{-1} can be attributed to the formation of the TiCN ternary compound (Escobar-Alarcón *et al* 2010). In addition, the spectrum shows significant D ('disorder', at about 1370 cm^{-1}) and G ('graphitic', at about 1580 cm^{-1}) peaks, which confirms the presence of a-C phase. In summary, the TiN/TiCN multilayer film is composed of crystalline grains and a-C phase.

AFM was carried out to quantitatively study the surface morphology of the TiN/TiCN multilayer film. Figure 5 shows a representative AFM image of the final surface after deposition of the multilayer. The mean grain size and the root-mean-square (RMS) roughness of the final surface TiCN layer are 8.0 nm and 10.8 nm by means of statistical analysis

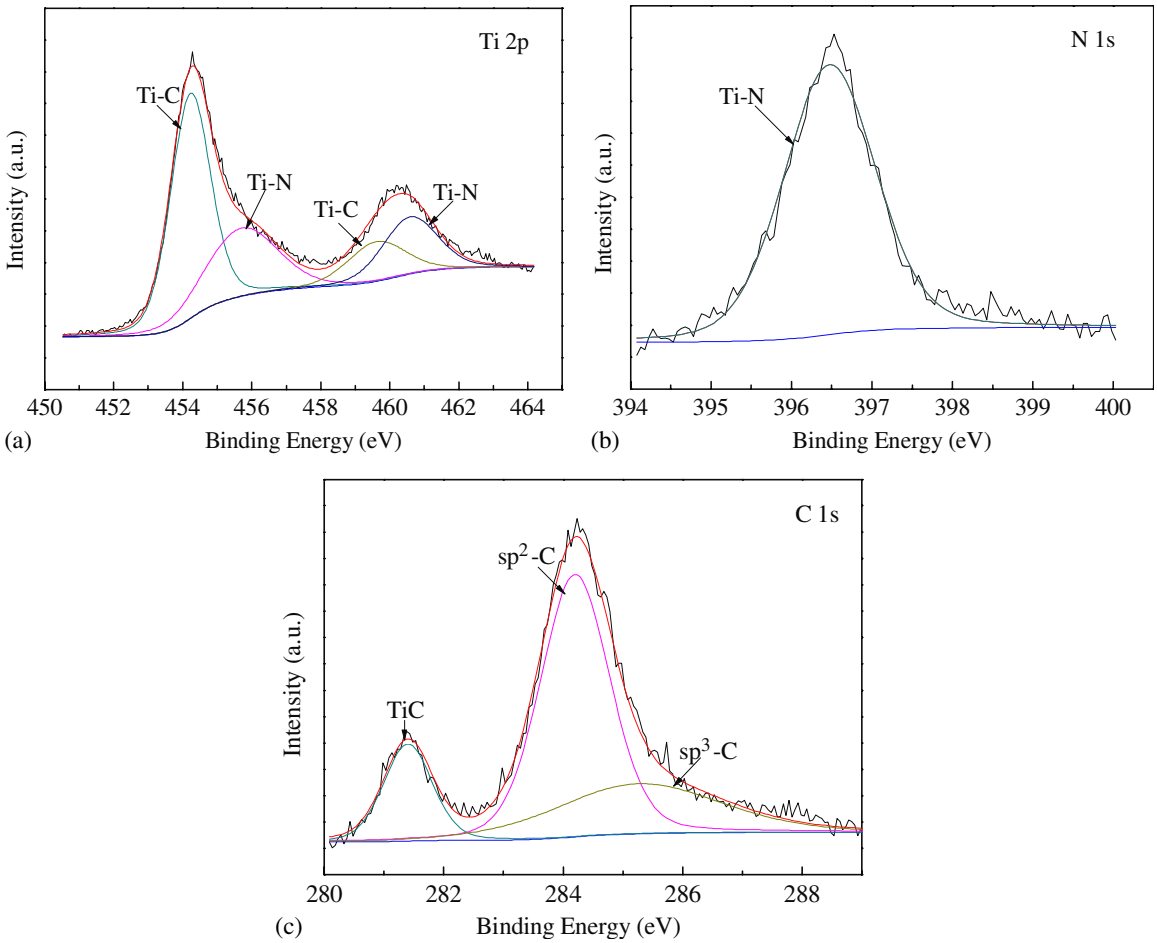

Figure 3. XPS spectra of Ti 2p, N 1s and C 1s for the film.

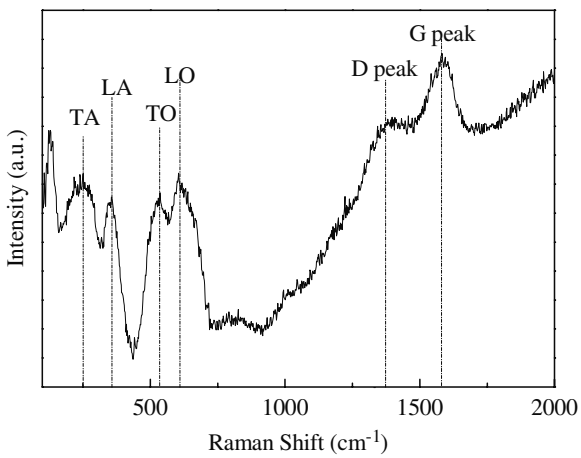

Figure 4. Raman spectrum of the TiN/TiCN multilayer film.

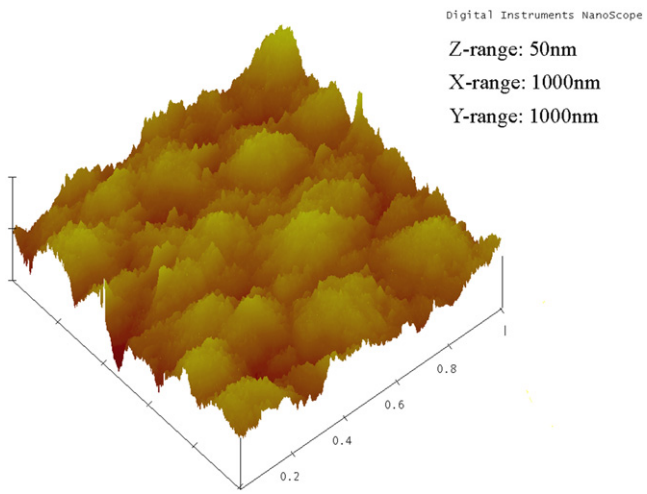

Figure 5. AFM images of the TiN/TiCN multilayer film.

and a scanning probe image processor (SPIP), respectively. However, the grain size of the final surface TiCN layer is different from the data of XRD. Many authors have reported this phenomenon and considered that the information obtained from XRD on crystal sizes is usually more reliable (Caicedo *et al* 2010).

In order to acquire the microstructure of the TiN/TiCN multilayer film, the fractured cross-section and the thickness of the films were determined by the FESEM technique. Figure 6 shows the FESEM images of the fractured cross-section of the multilayer film. As described in figure 6(*a*), the thicknesses of the total film and the uppermost TiCN layer are about 9675 nm and 1542 nm, respectively. Then the thickness of the bilayer, which includes around 500 nm TiCN layer and around 360 nm TiN layer, is about 860 nm when the bilayer

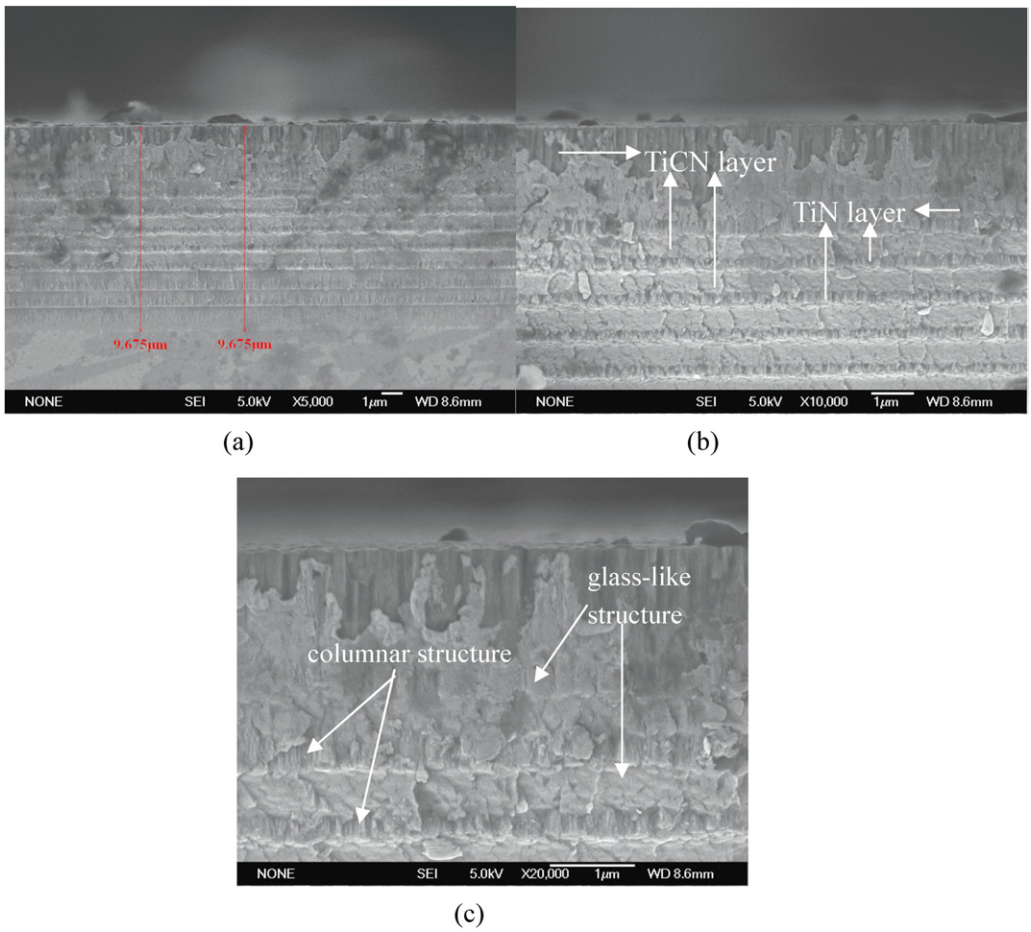

Figure 6. FESEM images of the fractured cross-section of the multilayer film: (*a*) ×5000, (*b*) ×10 000, (*c*) ×20 000.

number ranges from 2 to 9. On the basis of their thicknesses and deposition time, the deposition rates of the TiN layer and TiCN layer are about 110 nm min^{-1} and 100 nm min^{-1}, respectively. Furthermore, it can be found that there are glass-like and columnar structures within the film in figure 6(*c*). The glass-like structure is featureless and relatively smooth, which is different from the columnar structure. With respect to the formation of the glass-like structure, two important factors should be taken into account: (1) high deposition rate, which mainly depends on ion energy, (2) excessive C atoms. Firstly, the high deposition rate results in the suppression of crystal growth. Secondly, a supersaturated solid solution is formed by the excessive C atoms. Thus, these phenomena help in the formation of the glass-like structure.

It can be observed from figure 6(*b*) that in the inner film, except for the bottom part, the TiCN layers show a distinct glass-like structure and the TiN layers present the representative columnar structure. However, the uppermost TiCN layer exhibits some columnar crystal structure due to sufficient thickness compared with other TiCN layers. With the increase in the thickness of the uppermost TiCN layer, the stress increases in the layer (Abadias 2008), namely a high Gibbs free energy exists in the layer. In order to reduce the Gibbs free energy, the transition of the structure from glass-like to columnar is spontaneous. Moreover, in figure 6(*a*), the TiCN layer in the bottom part of the film also displays a slightly columnar structure. This can be attributed to the larger stress in the bottom part of the film than in the top part of the film. Additionally, no microcracks and delaminations can be observed between the film–substrate interface and layer–layer boundary of the film from figure 6(*b*). As a result, the multilayer film would exhibit good adhesion force and excellent wear resistance. To prove this, we carried out further studies as follows.

3.2. *Mechanical properties*

A scratch tester was used to obtain the adhesion force of the TiN/TiCN multilayer film. During the scratch test, the first crack or the primary flaking of films corresponds to the critical load. Figure 7 shows the scratch curve of the TiN/TiCN multilayer film. The value of critical load is about 37.8 N, i.e. the adhesion interface fails when the load is about 37.8 N. The scratch track corresponding to the critical load is presented in figure 8 observed by 3D surface profiler. The dark area is the Si substrate and the bright region is the film surface. It is showed that the film completely flaked away from the substrate. Furthermore, it could be concluded from figure 7 that the TiN/TiCN multilayer film failed by flaking rather than by cracking or delamination, which should be attributed to the columnar-like structure of the TiN layer (Qi *et al* 2010).

The nano-hardness of the TiN/TiCN multilayer film was measured by a nano-indenter. Figure 9 illustrates

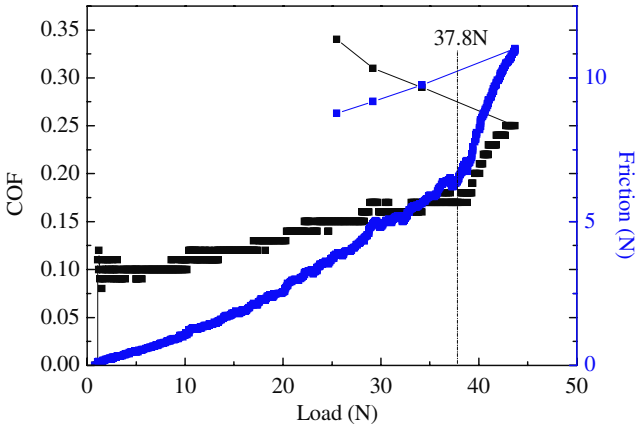

Figure 7. Scratch test curves of the TiN/TiCN multilayer film.

Figure 8. Micrograph of the scratch track with critical load.

the load–unloading curves of the TiN/TiCN multilayer film obtained from a Berkovich diamond indenter at a load of 280 mN. The hardness, the elastic modulus and the penetration depth of the total film and the uppermost layer are shown in table 3. It is easily found that the hardness of the uppermost layer is higher than that of the total film. The high hardness in the uppermost layer is attributed to the dislocation motion inhibited by the a-C and the glass-like structure (Kim *et al* 2003b). But, when the penetration depth reaches 900 nm, the hardness of the film is significantly influenced by the TiN layer. The TiN layer, which has a columnar structure, presents a relatively low hardness. Thus, the hardness of the total film decreases in contrast with that of the uppermost layer. It has been reported that the hardness values of TiN, TiCN and TiN/TiCN films are in the range from 17 GPa to 26 GPa (Peters and Nastasi 2002; Serro *et al* 2009), 17.5 GPa to 32.8 GPa (Escobar-Alarcón *et al* 2010) and 27 GPa to 36 GPa (Raveh *et al* 2007, Zukerman *et al* 2007), respectively. Therefore, in this work, the hardness of the TiN/TiCN multilayer film is satisfactory.

3.3. Tribological properties

The curves of coefficient of friction (COF) for the TiN/TiCN multilayer film against steel and Si_3N_4 balls are displayed in

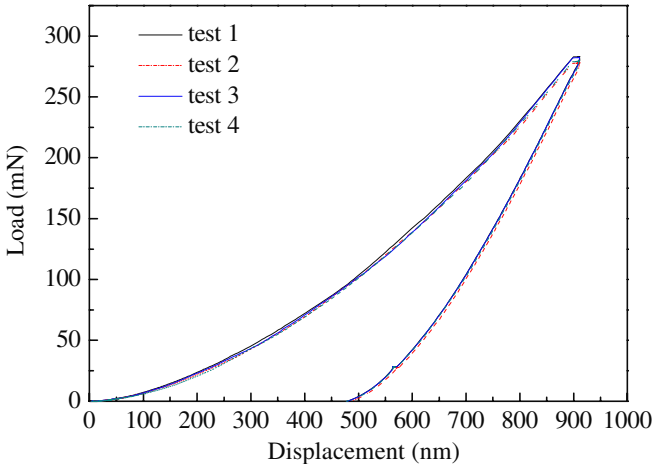

Figure 9. Load–displacement curves of the TiN/TiCN multilayer film.

Table 3. Nano-indentation test results for the film and the uppermost layer.

Sample	Mean hardness (GPa)	Mean elastic modulus (GPa)	Penetration depth (nm)
Total film	27.22	362.1	900
Uppermost layer	34.22	281.5	150

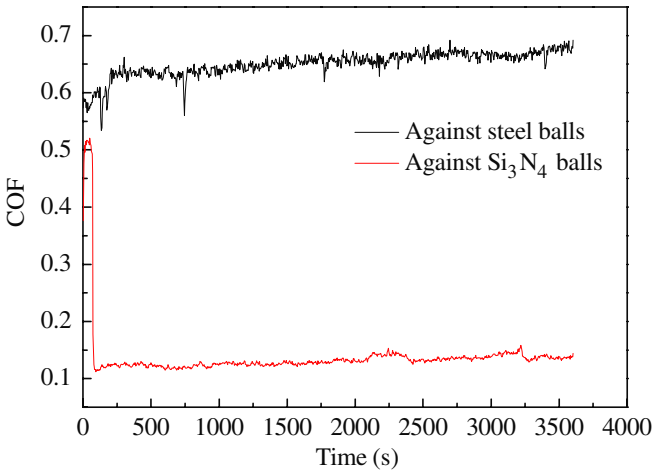

Figure 10. COF curves of the TiN/TiCN multilayer film against Si_3N_4 and steel balls.

figure 10. It is easily observed that the COF of the film is higher, about 0.65 in steady state when sliding against the steel balls. Accordingly, the wear track of the film against steel ball is shown in figure 11. It is unforeseen that the wear track on the film surface is very shallow and smooth but wide from figure 11(*a*), and the depth of the wear track is 560 nm from figure 11(*b*). According to equation (1), the wear rate is 2.49×10^{-6} mm^3 N^{-1} m^{-1}. In fact, Huang *et al* (2002) reported a result about a TiCN film with a low COF when the wear track is shallow and smooth. Nevertheless, the TiN/TiCN multilayer film against steel balls has a comparatively high COF. Aiming to study the peculiar phenomenon presented by the TiN/TiCN multilayer film, SEM micrograph and EDS analysis of the wear track for the film against steel balls were performed (see

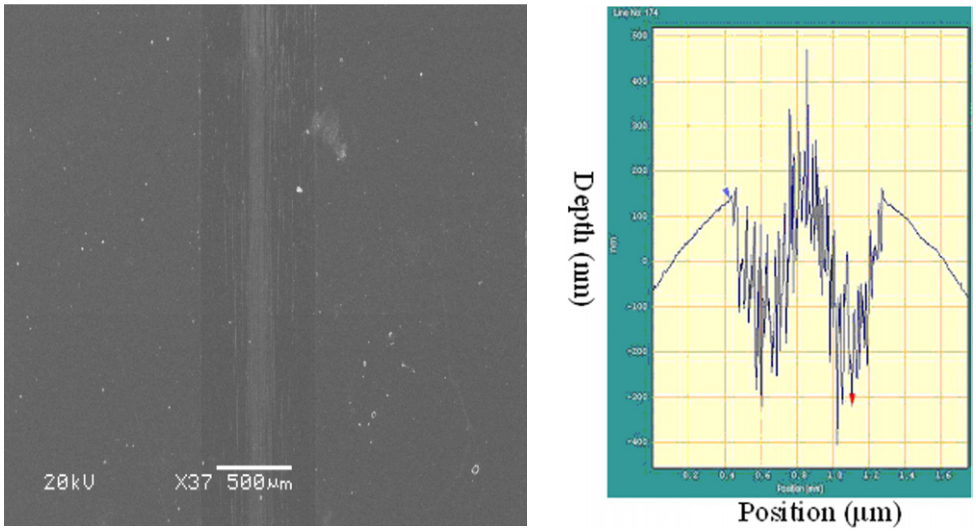

Figure 11. Wear track of the film against steel ball: (*a*) SEM micrograph ×37, (*b*) depth profile of wear track by 3D technology.

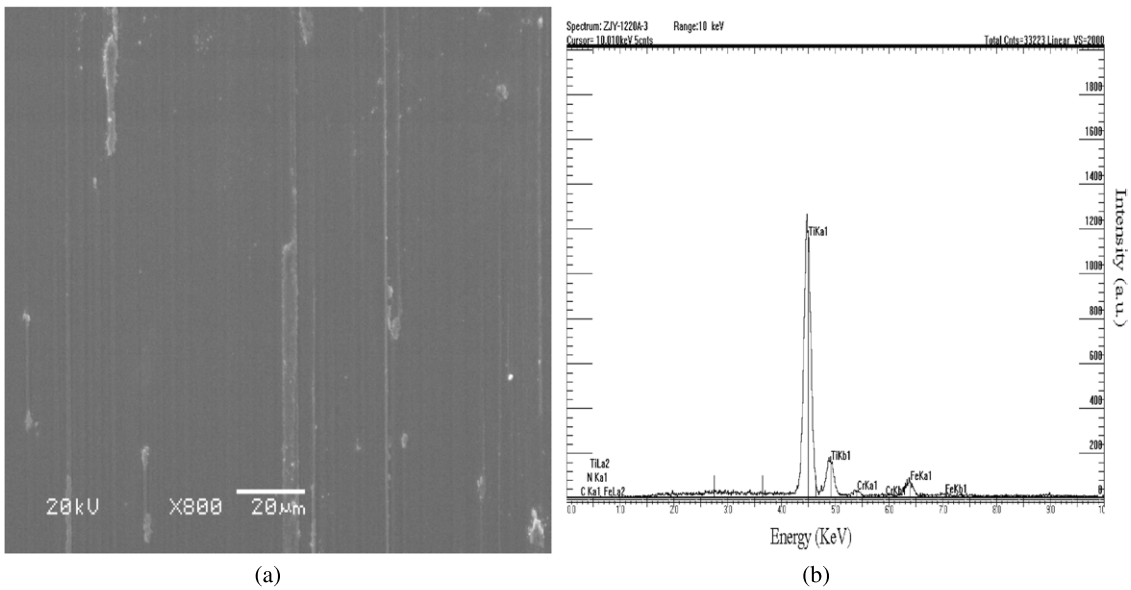

Figure 12. Wear track of the film against steel ball: (*a*) SEM micrograph ×800, (*b*) corresponding EDS analysis of (*a*).

figure 12), and there are some facts to explain it. Firstly, as shown in figure 12(*b*), Fe and Cr elements are detected on the wear track of the film. It could be speculated that Fe and Cr elements got transferred from the steel balls to the film surface. As a result, friction between steel and steel occurred during sliding, and the COF became higher physically. Other authors have also reported that the COF is about 0.5–0.7 when steel slides against steel balls (Foerster *et al* 2007, Guruvenket *et al* 2009, Wang *et al* 2010). Secondly, the wide wear track and the larger contact area cause a higher shear stress, and it results in a high COF (Su and Kao 2001). Thirdly, the lubricative transfer layer is discontinuous and rare in the wear track, as shown in figure 12(*a*). It can be implied that the film performs a barely satisfactory lubricative property when sliding against steel balls (de Figueiredo *et al* 2008). Finally, from figure 11, it is very possible that the abrasive dust produced between the frictional interface is trapped in the edges of the contact surface and plays the role of abrasive particles resulting in more rapid wear in the edges of the wear track than at the centre (Kester *et al* 1999). This is also a reason for the high COF.

However, the mean COF and the wear rate are about 0.14 and 1.15×10^{-6} mm^3 N^{-1} m^{-1} for the film against Si_3N_4 balls. As seen in figure 10, the total friction curve of the film against Si_3N_4 balls is steady and smooth with a short running-in period. In addition, the SEM micrographs and the 3D image of the wear track for the film against Si_3N_4 balls were recorded (see figure 13). Compared with the film against steel balls, the film against Si_3N_4 balls shows a low COF. The low COF can be attributed to the narrow wear track and the formation of transfer layer at the centre of the wear track, as shown in figures 13(*a*) and (*b*). The depth of the edges of the wear track exceeds 2000 nm and is deeper than that of the central region, as shown

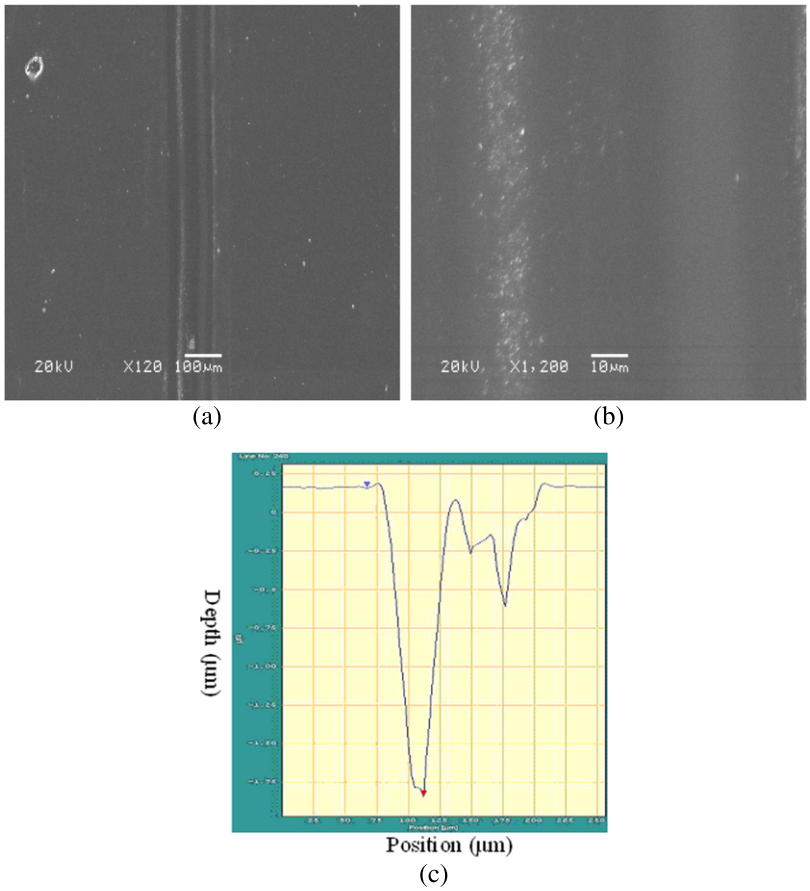

Figure 13. Wear track of the film against Si_3N_4 ball: (*a*) SEM micrograph ×120, (*b*) SEM micrograph ×1200, (*c*) depth profile of wear track by 3D technology.

in figure 13(*c*). It is indicated that the uppermost TiCN layer has worn out, but the Si_3N_4 balls cannot contact the TiN layer since the depth of the central region of the wear track is 100 nm. There are some facts to explain these phenomena. One reason for the large difference in height between the edge and the centre was explained in the previous section. The second reason is that the existence of the transfer layer contributes to a low mass loss of the central region of the wear track. The third reason may be that the hard debris trapped in the edges of the contact surface will suffer a violent squeezing action by a hard counterpart and their quantity will be higher in the case of a soft steel ball (Stanishevsky and Lappalainen 2000). This assumption can also respond to the fact that the wear track is deeper and narrower when the film slides against Si_3N_4 balls than steel balls.

In summary, the COF and wear rate for the film against Si_3N_4 balls are lower than against steel balls. Furthermore, the thick TiN/TiCN multilayer film exhibits good tribological behaviour for lengthening the service life.

4. Conclusions

A thick TiN/TiCN multilayer film was deposited by dc magnetron sputtering. The structure and properties of the film were studied. The following conclusions are drawn based on the results in this study:

(1) The TiN/TiCN multilayer film had a thickness of 9675 nm and bilayer number of 10. In the inner film, the TiCN layer exhibited a glass-like structure and the TiN layer presented a columnar structure. However, the uppermost TiCN layer exhibited some columnar crystal structure. The average crystal size of the uppermost TiCN layer was estimated to be 14.6 nm by XRD. The a-C phase was also detected in the uppermost TiCN layer.

(2) The adhesion force and hardness of the TiN/TiCN multilayer film were 37.8 N and 34.22 GPa, respectively.

(3) Within a sliding time of 1 h, the mean COF and wear rate for the film against steel balls were 0.65 and 2.49 × 10^{-6} mm^3 N^{-1} m^{-1}. In contrast, the mean COF and wear rate were about 0.14 and 1.15 × 10^{-6} mm^3 N^{-1} m^{-1} for the film against Si_3N_4 balls.

Acknowledgments

The authors are grateful to the National Nature Science Foundation of China (50905177) and the National 973 Project of China (2007CB607601) for financial support.

References

Abadias G 2008 Stress and preferred orientation in nitride-based PVD coatings *Surf. Coat. Technol.* **202** 2223–35

Agudelo L C, Ospina R, Castillo H A and Devia A 2008 Synthesis of Ti/TiN/TiCN coatings grown in graded form by sputtering dc *Phys. Scr.* **T131** 014006

Antunes R A, Rodas A C D, Lima N B, Higa O Z and Costa I 2010 Study of the corrosion resistance and *in vitro* biocompatibility of PVD TiCN-coated AISI 316L austenitic stainless steel for orthopedic applications *Surf. Coat. Technol.* **205** 2074–81

Barshilia H C, Surya Prakash M, Jain A and Rajam K S 2005 Structure, hardness and thermal stability of TiAlN and nanolayered TiAlN/CrN multilayer films *Vacuum* **77** 169–79

Bemporad E, Peechio C, De Rossi S and Carassiti E 2001 Characterization and hardness modelling of alternate TiN/TiCN multilayer cathodic arc PVD coating on tool steel *Surf. Coat. Technol.* **146** 363–70

Caicedo J C, Amaya C, Yate L, Gómez M E, Zambrano G, Alvarado-Rivera J, Muñoz-Saldaña J and Prieto P 2010 TiCN/TiNbCN multilayer coatings with enhanced mechanical properties *Appl. Surf. Sci.* **256** 5898–904

Chang Y-Y and Chang C-P 2009 Microstructural and mechanical properties of graded and multilayered $Al_xTi_{1-x}N$/CrN coatings synthesized by a cathodic-arc deposition process *Surf. Coat. Technol.* **204** 1030–4

Cheng Y H, Browne T and Heckerman B 2010 Influence of CH_4 fraction on the composition, structure, and internal stress of the TiCN coatings deposited by LAFAD technique *Vacuum* **85** 89–94

de Figueiredo M R, Neidhardt J, Kaindl R, Reiter A, Tessadri R and Mitterer C 2008 Formation mechanisms of low-friction tribo-layers on arc-evaporated $TiC_{1-x}N_x$ hard coatings *Wear* **265** 525–32

Escobar-Alarcón L, Camps E, Romero S, Muhl S, Camps I and Haro-Poniatowski E 2010 TiCN thin films grown by reactive crossed beam pulsed laser deposition *Appl. Phys.* A **101** 771–5

Foerster C E, Serbena F C, da Silva S L R, Lepienski C M, Siqueira C and Ueda M 2007 Mechanical and tribological properties of AISI 304 stainless steel nitrided by glow discharge compared to ion implantation and plasma immersion ion implantation *Nucl. Instrum. Methods* B **257** 732–6

Graca S, Carvalho P A and Colaco R 2011 Dislocation structures in nanoindented ductile metals—a transmission electron microscopy direct observation *J. Phys. D: Appl. Phys.* **44** 35402

Guruvenket S, Li D, Klemberg-Sapieha J E, Martinu L and Szpunar J 2009 Mechanical and tribological properties of duplex treated TiN, nc-TiN/a-SiN_x and nc-TiCN/a-SiCN coatings deposited on 410 low alloy stainless steel *Surf. Coat. Technol.* **203** 2905–11

Huang S W, Ng M W, Samandi M and Brandt M 2002 Tribological behaviour and microstructure of TiC(x)N((1-x)) coatings deposited by filtered arc *Wear* **252** 566–79

Irmer G and Dorner-Reisel A 2005 Micro-Raman studies on DLC coatings *Adv. Eng. Mater.* **7** 694–705

Jiang J L, Hao J Y, Pang X J, Wang P and Liu W M 2010 Structure and characteristics of amorphous (Ti,Si)-C:H films deposited by reactive magnetron sputtering *Diamond Relat. Mater.* **19** 1172–7

Kester D J, Brodbeck C L, Singer I L and Kyriakopoulos A 1999 Sliding wear behavior of diamond-like nanocomposite coatings *Surf. Coat. Technol.* **113** 268–73

Kim G S, Lee S Y, Hahn J H, Lee B Y, Han J G, Lee J H and Lee S Y 2003a Effects of the thickness of Ti buffer layer on the mechanical properties of TiN coatings *Surf. Coat. Technol.* **171** 83–90

Kim G S, Lee S Y, Hahn J H and Lee S Y 2003b Synthesis of CrN/AlN superlattice coatings using closed-field unbalanced magnetron sputtering process *Surf. Coat. Technol.* **171** 91–5

Klemberg-Sapieha J E, Jedrzejowski P and Martinu L 2007 Mechanical and optical characteristics of superhard nanocomposite TiN/a-Si_3N_4 and TiCN/a-SiCN coatings produced by PECVD *J. Superhard Mater.* **29** 147–52

Klug H P and Alexander L E 1974 *X-Ray Diffraction Procedures: For Polycrystalline and Amorphous Materials* (New York: Wiley-Interscience)

Louw C W, Strydom I L and van den Heever K 1991 Selective steam oxidation of titanium and aluminium in TiN and (Ti, Al)N physically vapour-deposited coatings on dental surgical tools *Surf. Coat. Technol.* **49** 348–52

Meng J, Lu J, Wang J and Yang S 2006 Tribological behavior of TiCN-based cermets at elevated temperatures *Mater. Sci. Eng.* A **418** 68–76

Miao Q, Cui C E and Pan J D 2007 CrN–TiN multilayer coating on magnesium alloy AZ91 by arc-glow plasma deposition process *Surf. Coat. Technol.* **201** 5077–80

Monaghan D P, Teer D G, Laing K C, Efeoglu I and Arnell R D 1993 Deposition of graded alloy nitride films by closed field unbalanced magnetron sputtering *Surf. Coat. Technol.* **59** 21–5

Morant C, Prieto P, Forn A, Picas J A, Elizalde E and Sanz J M 2004 Hardness enchancement by CN/TiCN/TiN multilayer films *Surf. Coat. Technol.* **180–181** 512–8

Ogwu A A, Lamberton R W, Maguire P D and McLaughlin J A 1999 The effect of the substrate bias on the Raman spectra and thermal stability of diamond-like carbon (DLC) and silicon-modified DLC films prepared by plasma-enhanced chemical vapour deposition (PECVD) *J. Phys. D: Appl. Phys.* **32** 981–7

Oh S M, Rhee B G and Jeong B S 2003 Wear behaviors of ceramics TiN, TiC and TiCN with arc ion plating *KSME Int. J.* **17** 1904–11

Peters A M and Nastasi M 2002 Effect of carrier gas on the deposition of titanium carbo-nitride coatings by a novel organo-metallic plasma immersion ion processing technique *Vacuum* **67** 169–75

Polcar T, Martinez R, Vítù T, Kopecký L, Rodriguez R and Cavaleiro A 2009 High temperature tribology of CrN and multilayered Cr/CrN coatings *Surf. Coat. Technol.* **203** 3254–9

Qi Z, Sun P and Wang Z 2010 *Proc. Int. Conf. on Technical Sessions (Beijing, China)* Part 3 (Berlin: Springer) pp 796–800

Raveh A, Zukerman I, Kalman H, Klemberg-Sapieha J E and Martinu L 2007 Thermal stability and wear resistance of hard TiN/TiCN coatings on plasma nitrided PH15-5 steel *Wear* **263** 1249–52

Serro A P, Completo C, Colaço R, dos Santos F, da Silva C L, Cabral J M S, Araújo H, Pires E and Saramago B 2009 A comparative study of titanium nitrides, TiN, TiNbN and TiCN, as coatings for biomedical applications *Surf. Coat. Technol.* **203** 3701–7

Shi Y L, Peng H R, Xie Y, Xie G W, Zhao C and Li S Z 2000 Plasma CVD of hard coatings Ti(CNO) using metallo-organic compound Ti(OC3H7)(4) *Surf. Coat. Technol.* **132** 26–30

Stanishevsky A and Lappalainen R 2000 Tribological properties of composite Ti(N,O,C) coatings containing hard amorphous carbon layers *Surf. Coat. Technol.* **123** 101–5

Su Y L and Kao W H 2001 Tribological behavior and wear mechanisms of Ti-C:H/TiC/TiCN/TiN/Ti coatings when sliding against steel, bronze and aluminum alloy rods *J. Mater. Sci.* **36** 189–99

Tu J P, Chen R, Liu D G, Mai Y J and Gu C D 2011 Microstructure, mechanical and tribological properties of TiCN nanocomposite films deposited by dc magnetron sputtering *Surf. Coat. Technol.* **205** 5228–34

Wang L, Ma J Q, Yang J, Bi Q L, Fu L C and Liu W M 2010 Dry-sliding tribological properties of a nano-eutectic $Fe_{1.87}C_{0.13}$ alloy *Wear* **268** 991–5

Zukerman I, Raveh A, Landau Y, Weiss R, Shneck R, Shneor Y, Kalman H, Klembergsaphieha J and Martinu L 2007 Tribological properties of duplex treated TiN/TiCN coatings on plasma nitrided PH15-5 steel *Surf. Coat. Technol.* **201** 6171–5